Review Article

Journal of Molecular Microbiology and Biotechnology

J Mol Microbiol Biotechnol 2016;26:76–91
DOI: 10.1159/000440882

Published online: March 10, 2016

Structure and Function of 4-Hydroxyphenylacetate Decarboxylase and Its Cognate Activating Enzyme

Brinda Selvaraj[a, e] Wolfgang Buckel[b, c] Bernard T. Golding[f]
G. Matthias Ullmann[d] Berta M. Martins[a]

[a]Institut für Biologie, Strukturbiologie/Biochemie, Humboldt-Universität zu Berlin, Berlin, [b]Fachbereich Biologie und Synmikro, Philipps-Universität, and [c]Max-Planck-Institut für terrestrische Mikrobiologie, Marburg, [d]Computational Biochemistry, BGI, Universität Bayreuth, Bayreuth, Germany; [e]Department of Medical Biochemistry and Biophysics, Karolinska Institutet, Stockholm, Sweden; [f]School of Chemistry, Newcastle University, Newcastle upon Tyne, UK

Key Words

Aromatic degradation · 4-Methylphenol · Cresol · S-adenosylmethionine · Glycyl radical enzymes · Fe-S cluster · C-C bond cleavage · Radical catalysis

Abstract

4-Hydroxyphenylacetate decarboxylase (4Hpad) is the prototype of a new class of Fe-S cluster-dependent glycyl radical enzymes (Fe-S GREs) acting on aromatic compounds. The two-enzyme component system comprises a decarboxylase responsible for substrate conversion and a dedicated activating enzyme (4Hpad-AE). The decarboxylase uses a glycyl/thiyl radical dyad to convert 4-hydroxyphenylacetate into *p*-cresol (4-methylphenol) by a biologically unprecedented Kolbe-type decarboxylation. In addition to the radical dyad prosthetic group, the decarboxylase unit contains two [4Fe-4S] clusters coordinated by an extra small subunit of unknown function. 4Hpad-AE reductively cleaves S-adenosylmethionine (SAM or AdoMet) at a site-differentiated $[4Fe\text{-}4S]^{2+/+}$ cluster (RS cluster) generating a transient 5′-deoxyadenosyl radical that produces a stable glycyl radical in the decarboxylase by the abstraction of a hydrogen atom. 4Hpad-AE binds up to two auxiliary [4Fe-4S] clusters coordinated by a ferredoxin-like insert that is C-terminal to the RS cluster-binding motif. The ferredoxin-like domain with its two auxiliary clusters is not vital for SAM-dependent glycyl radical formation in the decarboxylase, but facilitates a longer lifetime for the radical. This review describes the 4Hpad and cognate AE families and focuses on the recent advances and open questions concerning the structure, function and mechanism of this novel Fe-S-dependent class of GREs.

Introduction

The decarboxylation of 4-hydroxyphenylacetate to *p*-cresol or the dehydration of glycerol to 3-hydroxypropanal are two examples of several reactions that cannot proceed by ionic mechanisms with carbanions as intermediates. In the anaerobic world, the bioconversion of such recalcitrant substrates is promoted by using radical intermediates [Buckel, 2009]. Glycyl radical enzymes (GREs) are versatile biocatalysts that use a radical dyad prosthetic group comprising a glycine residue (as radical

KARGER

E-Mail karger@karger.com
www.karger.com/mmb

1464–1801/16/0263–0076$39.50/0

Dr. Berta M. Martins
Institut für Biologie, Strukturbiologie/Biochemie
Humboldt-Universität zu Berlin, Unter den Linden 6
DE–10099 Berlin (Germany)
E-Mail berta.martins@hu-berlin.de

storage site) and a neighbouring cysteine [Frey et al., 2006]. GREs can stabilize the glycyl radical within the protein matrix and recycle it after an enzymatic turnover [Hioe et al., 2011].

Functional GREs are generated via post-translational activation by a specific activating enzyme (AE) belonging to the S-adenosylmethionine (SAM or AdoMet)-dependent radical superfamily [Shisler and Broderick, 2014; Sofia et al., 2001]. The AEs use a site-differentiated SAM-binding [4Fe-4S] cluster coordinated by three cysteines with one accessible iron (RS cluster) to catalyse the reductive cleavage of SAM to methionine and a transient 5′-deoxyadenosyl radical. This radical stereospecifically abstracts a hydrogen atom from a glycine residue in the C-terminus of the cognate GRE, generating a glycyl radical [Selmer et al., 2005; Shisler and Broderick, 2014]. Once activated, GREs are kept in a dormant state (radical storage form) and only upon substrate binding does the glycyl radical generate a polypeptide-bound thiyl radical within a neighbouring cysteine [Eklund and Fontecave, 1999]. Such thiyl radicals usually activate a substrate molecule by hydrogen atom abstraction, although besides addition to a carbonyl group, oxidation of an anion or other chemical transformation can occur [Frey et al., 2008]. The catalytic pathway then proceeds via intermediate radicals until the product is formed and the thiyl radical is regenerated. The thiyl radical may either initiate a new catalytic cycle or, in the absence of substrate, re-abstract a hydrogen atom from the glycine to yield the storage glycyl radical.

GREs display a variety of reaction types. Examples are the scission or formation of C-C bonds catalyzed by pyruvate formate lyase (Pfl; E.C. 2.3.1.54) in anaerobic glucose fermentation, 4-hydroxyphenylacetate decarboxylase (4Hpad; E.C. 4.1.1.83) in the fermentation of tyrosine to *p*-cresol, and benzylsuccinate synthase (BSS; E.C. 4.1.99.11) in toluene degradation. Other examples are substitutions of oxygen and nitrogen by hydrogen in C-O or C-N-bonds catalyzed by class III ribonucleotide reductase (Nrd; E.C. 1.17.4.2), glycerol dehydratase (GD; E.C. 4.2.1.30) and choline trimethylamine lyase (CutC; E.C. 4.3.99.4). 4Hpad and BSS are structurally more complex GREs with extra small subunits essential for catalysis that bind Fe-S clusters: 4Hpad has one additional small subunit binding two [4Fe-4S] clusters [Martins et al., 2011; Yu et al., 2006] and BSS has two additional small subunits each binding one [4Fe-4S] cluster [Funk et al., 2014; Leuthner et al., 1998]. The respective AEs also display additional Fe-S clusters bound within a ferredoxin-like insert that is C-terminal to the RS cluster-binding motif. Except for the Pfl and Ndr systems, all GRE-AEs possess a similar ferredoxin-like domain. Auxiliary Fe-S clusters are widespread among radical SAM enzymes. Their proposed functions are still under debate and include the following: contributor to structural integrity, involvement in catalysis by substrate anchoring and conduit for electron transfer to the RS cluster [Lanz and Booker, 2012; Shisler and Broderick, 2014].

Current understanding is still poor as to how the Fe-S GRE family generates the SAM-dependent glycyl radical and regulates the reactivity of the glycyl/thiyl dyad radical. Moreover, the functional roles of the additional small subunit(s) with Fe-S clusters in the catalytic components and the auxiliary Fe-S cluster(s) present in the AEs are not completely understood. Recent studies have provided significant insights into the structure and function of 4Hpad and BSS, and by combining biochemical with structural and theoretical analyses, there is now a fairly good mechanistic picture of the processes involved in activation and substrate conversion. See the article from Heider et al. [this issue, pp. 29–44] in the same issue for a detailed review on BSS. This review focuses on recent progress in the molecular mechanisms of 4Hpad activation and substrate conversion.

Occurrence and Biological Function of the 4Hpad System

The two-enzyme component system 4Hpad/4Hpad-AE catalyses the final step in the fermentation of tyrosine to *p*-cresol in several facultative and obligately anaerobic bacteria. *p*-Cresol formation from tyrosine was first reported in 1949 [Stone et al., 1949]. In the 1970's *Clostridium difficile* and *Clostridium scatologenes* were shown to produce *p*-cresol with *p*-hydroxyphenylacetate as the immediate precursor [Elsden et al., 1976]. Subsequently, *p*-cresol formation by decarboxylation of *p*-hydroxyphenylacetate was reported for *Lactobacillus* strains [Yokoyama and Carlson, 1981] and for cell-free extracts of *C. difficile* [D'Ari and Barker, 1985].

Biological Relevance of p-Cresol

p-Cresol (4-methylphenol) is commonly found in nature. Natural sources range from coal tar, petroleum and wood, to pheromones and animal manure (*p*-cresol is the major component responsible for its odour), to wines and beers. Dominant anthropogenic sources are plastics, pharmaceuticals, herbicides, antioxidants, agrochemicals and dyes (Agency for Toxic Substances and Disease Reg-

Table 1. Currently annotated/putative non-redundant sequences (>45% sequence identity) for the *p*-hydroxyphenylacetate decarboxylase catalytic subunit from *C. scatologenes*

Organism	Locus and length, aa	Accession	Sequence identity, %
C. scatologenes	Q38HX4 897	gi:122577961	100
Clostridium drakei	WP_032075373 897	gi:692119105*	99
Clostridium carboxidivorans	WP_007061353 897	gi:494121576*	98
Peptostreptococcaceae bacterium VA2	WP_026900837 897	gi:652506528*	84
Holophaga foetida	WP_005035449 897	gi:491177083*	82
Clostridium diolis	WP_039773512 897	gi:748202607*	83
Sedimentibacter sp. B4	WP_019229290 905	gi:518059082*	79
Multispecies *Blautia*	WP_005952614 897	gi:492756463*	80
Clostridiales bacterium VE202-21	WP_025655707 898	gi:647170587*	77
Clostridium sp. CAG:505	WP_022364219 898	gi:547964054*	78
Collinsella sp. CAG:289	WP_022386687 902	gi:548164480 formate C-acetyltransferase	68
Olsenella uli	WP_013251893 902	gi:503016917*	68
P. difficile	WP_009895226 902	gi:97581042	58
Candidatus C. anorexicamassiliense	WP_040327801 895	gi:749944998*	57
Clostridium lundense	WP_027623090 905	gi:653612614*	57
Arsenophonus endosymbiont of *Nilaparvata lugens*	WP_032115537 898	gi:692119105*	56
Clostridium botulinum	WP_017352501 905	gi:515921918*	57
Pelosinus sp. UF01	WP_038673622 900	gi:740888374*	55
Carnobacterium sp. N15.MGS-207	WP_046430676 904	gi:815697119*	55
Phascolarctobacterium sp. CAG:207	WP_021717278 904	gi:545588516*	55
Succinispira mobilis	WP_019878801 904	gi:518718033 hypothetical protein	53
Tannerella forsythia	WP_014223608 903	gi:503989614*	54
T. forsythia 3313	BAR47717 903	gi:806916713 pyruvate formate-lyase	54
Atopobium rimae	WP_040324494 909	gi:749938628*	50
A. rimae ATCC 49626	EE17375 911	gi:221184984 pyruvate formate-lyase	50
Anaeroarcus burkinensis	WP_027938505 902	gi:654468116*	48
Blautia hydrogenotrophica CAG:147	WP_021845592 907	gi:546358547 hypothetical protein	49
*Chlamydia trachomatis***	CRH61180 818	gi:815103565	27
*Klebsiella pneumoniae***	AIT02791 765	gi:695175699	27
E. coli PMV-1**	YP_008574072 765	gi:544578548	29

aa = Amino acid sequence information.
* Annotated as major facilitator superfamily transporter. ** Most probably falsely annotated. See text for details.

istry: www.atsdr.cdc.gov). The molecule has a 'Janus-face' character, on the one hand being beneficial to health by virtue of its use in pharmaceuticals and in traps for malaria-transmitting insects. But the deleterious side of *p*-cresol is overwhelming. The human pathogen *Peptoclostridium difficile* (previous name *C. difficile*) produces *p*-cresol and can survive in media containing up to 0.4% of the bacteriostatic agent, thus allowing the pathogen to thrive under competitive conditions [Hafiz and Oakley, 1976]. In humans, *p*-cresol can be metabolized to *p*-cresol *o*-sulphate and to a lesser extend to *p*-cresol glucuronide, two uremic toxins implicated in chronic kidney disease [Bammens et al., 2006; Poveda et al., 2014]. As a consequence, the bacteriostatic property of *p*-cresol transforms a common and mostly non-lethal nosocomial *P. difficile* infection into a medical and economic problem, similar to methicillin-resistant *Staphylococcus aureus* [Dawson et al., 2008].

Amino Acid Sequence Information for the Decarboxylase Component 4Hpad

Currently, there are several putative homologues of the catalytic subunit of the decarboxylase from *C. scatologenes* (UniProt accession code Q38HX4, gi:656214192) annotated in the genomes of various bacteria listed in table 1. The entries are based on a non-redundant BLASTP 2.2.31 search [Altschul et al., 1997]. Three homologues (marked with double asterisk) are most probably wrongly annotated as *p*-hydroxyphenylacetate decarboxylases because the catalytic relevant amino acids, except for the radical-bearing cysteine and the neighbouring glutamate (C503 and E505; numbering from *C. scatologenes*), are not conserved: R223H, S344H, F405Y, H536S and E637Q.

Molecular Characterization of the 4Hpad System

Biochemistry and Spectroscopy Studies on the Decarboxylase and AE

Already in 1985, D'Ari and Barker [1985] postulated that at least two proteins are required for decarboxylation of *p*-hydroxyphenylacetate with one being necessary for keeping the decarboxylase continuously reduced and fully active. However, their high sensitivity to O_2 hindered the isolation of the proteins. In 2001, Selmer and Andrei [2001] isolated the decarboxylase for the first time from *P. difficile* and initially characterized it under strictly anoxic conditions. SDS-PAGE and size exclusion chromatography revealed that the native decarboxylase was a ho-

modimer of about 100 kDa per subunit. The identity of the protein was confirmed by N-terminal sequencing and screening against the unfinished genome sequence from *C. difficile* strain 630 (epidemic type X). The high-score ORF coded for a 902 amino acid protein with a predicted molecular mass of 101,294 Da and corroborated the value obtained for the purified protein. A PIR BLAST search produced several hits with Pfl-like proteins of unknown function indicating the decarboxylase was a member of the GRE family. As typical for GREs, an ORF coding the cognate AE (*hpd*A) was found downstream of the decarboxylase gene (*hpd*B), at a distance of 226 bp. A third ORF (*hpd*C) was found downstream of the *hpd*B gene, but its translated sequence did not show similarities to any protein of known function. There were several difficulties in extracting the protein from cell-free extracts, although it was possible to isolate the protein in an active state in the presence of sodium sulphide. The purified enzyme was specific for 4-hydroxyphenylacetate and 3,4-hydroxyphenylacetate (K_m of 2.8 mM and 0.5 mM, respectively) and was competitively inhibited by the substrate analogues 4-hydroxyphenylacetamide and 4-hydroxymandelate (apparent K_i of 0.7 mM and 0.48 mM, respectively) [Selmer and Andrei, 2001]. At the time it was unclear whether a low molecular mass cofactor responsible for enzyme activity in vivo was lost during the purification process. The missing cofactor was later identified as being a 9.5-kD small protein when the complete genome became available and the sequence of the putative operon showed that the third ORF *hpdC* is located between *hpdB* and *hpdA* [Andrei et al., 2004]. Due to its low molecular mass (9.5 kDa) compared with 100 kDa of *hpdB*, the small protein was overlooked on SDS-PAGE. Thus, the decarboxylase comprised two subunits: a catalytic one (β-subunit) with 100 kDa and a smaller one (γ-subunit) of 9.5 kDa of unknown function. This was in contrast to Pfl and class III Nrd containing only one catalytic subunit but similar to BSS with two additional small subunits [Selmer et al., 2005]. Selmer and Andrei [2001] cloned and expressed the genes of the decarboxylase *(hpdB* and *hpdC)* and the AE *(hpdA)* in *Escherichia coli*. The decarboxylase was purified as a hetero-octameric ($\beta_4\gamma_4$) catalytically competent complex, which could be activated by either the endogenous AE from *P. difficile* or the recombinant AE. The γ-subunit was essential for catalysis in vivo, as soluble decarboxylase could only be produced by the coexpression of both *hpdB* and *hpdC*. Reversible phosphorylation of the β-subunit was proposed to regulate the oligomeric state and decarboxylation activity of 4Hpad. Absorption spectroscopy and chemical analysis indicated the presence of iron-sulphur clusters in addition to the glycyl radical prosthetic group, but the function of these clusters remained elusive [Andrei et al., 2004]. In 2006, the decarboxylase and AE from *C. scatologenes* were produced in *E. coli* and characterized [Yu et al., 2006]. EPR spectroscopy corroborated the presence of two [4Fe-4S] clusters in the γ-subunit. These clusters were proposed to be responsible for the radical dissipation of previously activated enzymes in the absence of substrate.

As for 4Hpad-AE, SAM binds to the oxidized RS cluster with an affinity (23 ± 7 μM) [Selvaraj et al., 2013] similar to that observed for Pfl-AE (5.2 μM, aerobic studies) [Wong et al., 1993] and Ndr-AE (10 μM) [Ollagnier et al., 1997]. The K_d values are at least one order of magnitude below the physiological concentration of SAM (0.18–1 mM) [Bennett et al., 2009], indicating a high level of active-site saturation. In vivo studies with Pfl-AE suggested that the binding of AMP to the RS cluster protects it from oxidative damage during aerobic growth [Yang et al., 2009]. Such a protective mechanism might not be needed in strict anaerobes, which might explain why AMP binding to the RS cluster of isolated 4Hpad-AE was not detected [Selvaraj et al., 2013].

4Hpad-AE shares the conserved RS cluster CX_3CX_2C motif *(motif I)* at the N-terminus of the protein, but displays an additional cysteine-rich motif ($CX_{2-5}CX_{2-4}$-CX_{2-3}C-gap-C) within an insert of 50–60 amino acids that is C-terminal to the RS cluster motif [Yu et al., 2006]. With the exception of Pfl-AE [Knappe et al., 1984] and Nrd-AE [Gambarelli et al., 2005], all other identified homologues (Pfam: PF04055) have a similar ferredoxin-like domain, suggesting that the presence of additional [4Fe-4S] clusters is a common theme in the GRE-AEs [Selmer et al., 2005]. The number, composition and function of these clusters remained unknown. Absorption and EPR spectroscopy, as well as the iron content, confirmed the presence of two additional [4Fe-4S] clusters in 4Hpad-AE. These clusters were proposed to be involved in the electron transfer to the RS cluster, but seemed not to be directly involved in reductive cleavage of SAM [Yu et al., 2006].

Putative Role for the Ferredoxin-Like Domain in GRE-AEs

In recent years several SAM radical enzymes have been characterized and it is now clear that such auxiliary Fe-S clusters are widespread, with proposed tasks including the maintenance of structural integrity, the provision of an electron conduit to the RS cluster or direct involvement in catalysis by substrate anchoring [Lanz and Booker, 2012;

Shishler and Broderick, 2014]. With very few known exceptions, radical SAM enzymes use a $[4Fe\text{-}4S]^{2+/+}$ cluster coordinated by three cysteines with one accessible iron (RS cluster) to catalyse the homolytic cleavage of SAM into methionine and a transient 5′-deoxyadenosyl radical [Eklund and Fontecave, 1999; Frey et al., 2008; Shishler and Broderick, 2014]. The auxiliary clusters present in GRE-AEs have been postulated to be responsible for an alternative reductive cleavage of SAM as catalysed by the AE of GD (GD-AE) [Demick and Lanzilotta, 2011]. Namely, the authors claimed that GD-AE reductively cleaves SAM into 5′-deoxy-5′-methylthioadenosine and a 3-amino-3-carboxypropyl radical, but not into methionine and the 5′-deoxyadenosyl radical as catalysed by Pfl-AE [Dey et al., 2011] and Ndr-AE [Gambarelli et al., 2005], the only two known GRE-AEs without auxiliary clusters [Selmer et al., 2005]. Although Demick and Lanzilotta [2011] show the apparent but not convincing formation of low amounts of 5′-deoxy-5′-methylthioadenosine (fig. 3 in their paper), 2-aminobutyrate, the quenched 3-amino-3-carboxypropyl radical, was present in the assay mixture before the addition of the enzymes (fig. S2 in their paper). Hence the experiments with GD-AE need to be repeated. 4Hpad-AE uses the RS cluster to reductively cleave SAM into methionine and a transient 5′-deoxyadenosyl radical that directly activates the decarboxylase by hydrogen atom abstraction, as seen by the correlated formation of 5′-deoxyadenosine (5′-deoxyadenosyl radical quenched form) and glycyl radical [Selvaraj et al., 2013]. Thus, 4Hpad-AE containing auxiliary clusters does not follow the aforementioned postulated alternative SAM cleavage mechanism [Demick and Lanzilotta, 2011]. Instead, 4Hpad-AE catalyses a classical SAM-dependent glycyl radical formation, as reported for GR-AEs without auxiliary clusters [Dey et al., 2011; Gambarelli et al., 2005]. Currently, there is no information on which reaction path is followed by the AEs of BSS and choline trimethylamine lyase.

As the auxiliary clusters are not required for effective reductive cleavage of SAM at the RS cluster, the question remains as to what are the putative auxiliary [4Fe-4S] clusters from 4Hpad-AE good for? The cysteine-rich insert downstream of the RS cluster binding motif *(motif I)* can be divided into two motifs: $C56X_5C62X_2C65X_3C69$*(motif II)*-gap-$C89X_2C92X_4C97X_3C101$*(motif III)*-gap-C109 (numbers from UniProt accession code Q38HX2). Motifs II and III are similar to the cluster-binding motifs in 2×[4Fe-4S] ferredoxins (8Fe-Fd; Pfam: PF00037; fig. 1a). Hence, the putative auxiliary clusters in 4Hpad-AE and in other GRE-AEs could have a cysteinyl-crossed coordination, as seen in 8Fe ferredoxins. However, in the absence of structural information, it is difficult to pinpoint the exact pattern of coordination. How pivotal the knowledge on stoichiometry and configuration of a protein-bound cluster is to explain its function has recently been shown by the crystal structure of the 2-deoxy-scyllo-inosamine dehydrogenase from *Bacillus circulans*, a SAM radical enzyme displaying an unexpected coordination for the auxiliary clusters [Goldman et al., 2013]. The substrate 2-deoxy-scyllo-inosamine is located between the RS cluster and the auxiliary cluster. It is proposed that the 5′-deoxyadenosyl radical oxidizes the substrate's 3-hydroxyl group to a ketyl radical anion and the auxiliary cluster accepts the second electron to yield the ketone.

In the absence of structural information on 4Hpad-AE, a structure-based sequence alignment with Pfl-AE (PDB code 3C8F) [Vey et al., 2008] was used to design a truncated version of 4Hpad-AE lacking the ferredoxin-like domain, comprising *motif II* and *motif III* (Δ66-AE; fig. 1b, c).

Δ66-AE was remarkably stable. EPR and Mössbauer spectroscopy confirmed the presence of an expected $[4Fe\text{-}4S]^{2+/+}$ RS cluster [Selvaraj et al., 2014]. The environment of the RS cluster is not substantially affected by the deletion of the ferredoxin-like domain as only small differences were observed for SAM reactivity and binding affinity. Namely, the rate for reductive cleavage of SAM was 0.13–0.19 min^{-1} for Δ66-AE [Selvaraj et al., 2014] compared with 0.19 min^{-1} for WT-AE [Selvaraj et al., 2013], whilst K_d = 124 μM for Δ66-AE (Selvaraj et al., 2014) compared with K_d = 23 μM for WT-AE [Selvaraj et al., 2013]. Like WT-AE, Δ66-AE is also able to activate the decarboxylase within 2 min of incubation and the yield for glycyl radical formation is slightly decreased (30% less). But the generated radical decays considerably faster ($t_{1/2}$ = 5 min) compared with activation with WT-AE ($t_{1/2}$ >30 min) [Selvaraj et al., 2014]. Thus, although not required for SAM-dependent glycyl radical generation in the decarboxylase, the ferredoxin-like domain is necessary for producing a persistent radical. In the absence of structural information one can only guess which molecular mechanisms are responsible for the observed radical stabilization effect.

The mechanism of activation of GREs via their cognate GRE-AEs is an open question. Because the glycyl radical is recycled after each catalytic turnover, only stoichiometric amounts of the transient 5′-deoxyadenosyl radical are sufficient for activation [Eklund and Fontecave, 1999; Shisler and Broderick, 2014]. Hence, a stable complex between GRE and its cognate AE is counterproductive as it might inhibit the binding of the substrate or the release of the product. The only available structural

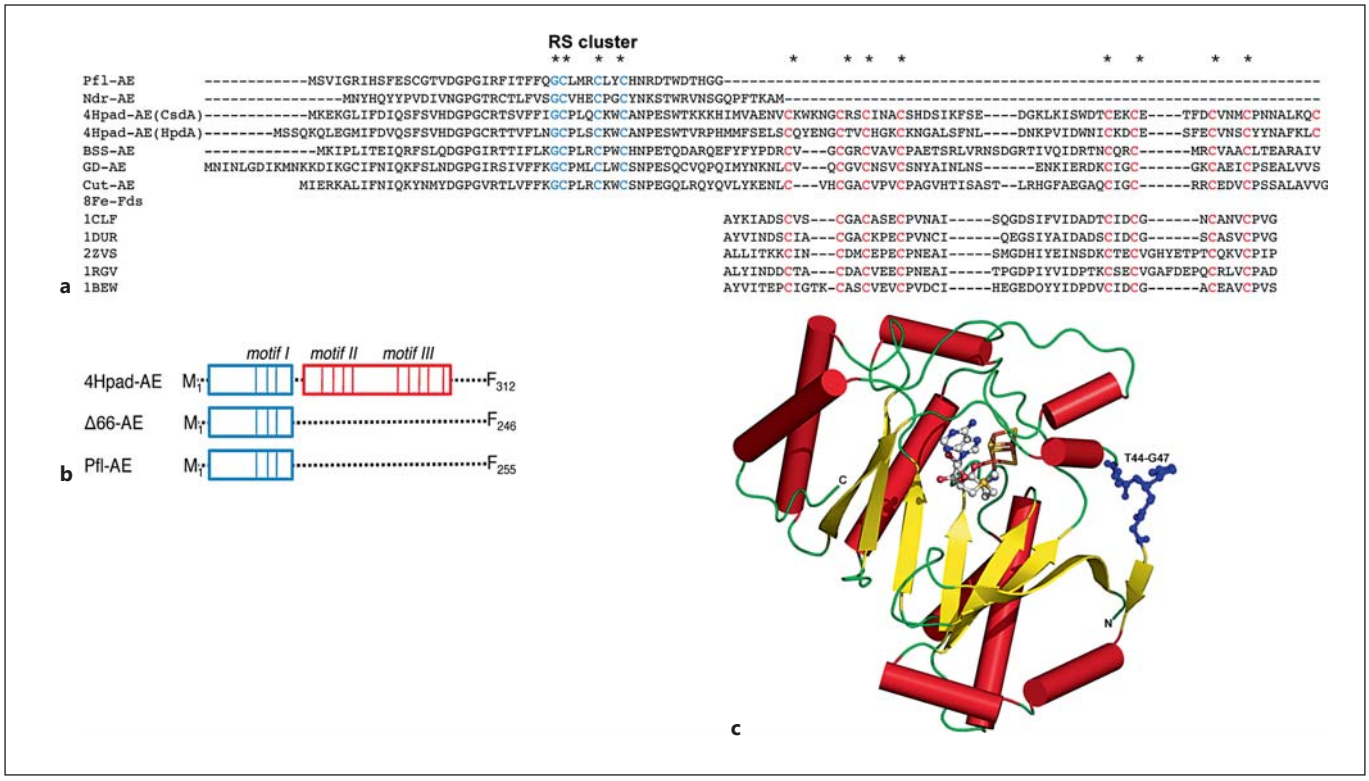

Fig. 1. Putative ferredoxin-like domain in GRE-AEs. **a** Multiple amino acid sequence alignment of N-terminal regions from 4Hpad-AE, known GRE-AEs and 8Fe ferredoxins (8Fe-Fds). Asterisks indicate binding motifs of conserved Fe-S clusters. The RS cluster-binding motif (GCX_3CX_2C) is coloured in blue. Other conserved cysteines are coloured in red. Accession codes for GREs are as follows: Pfl-AE (AAC73988), Ndr-AE (EPH54183), 4Hpad-AE (Csd*A*; *C. scatologenes*; ABB05048), 4Hpad-AE (Hpd*A*; *P. difficile*; WP_009888001), BSS-AE (AAK50370), GD-AE (AAM54729) and Cut-AE (ABB40075). For 8Fe ferredoxins the amino acid sequences were retrieved from the respective Protein Data Bank entry. **b** Scheme representing the amino acid sequence motifs I to III of wild-type 4Hpad-AE, of the 4Hpad-AE variant lacking the ferredoxin-like domain (Δ66-AE) and of Pfl-AE. The blue box represents motif I with cysteines coordinating the RS cluster shown as bars. The red box represents the ferredoxin-like domain with cysteines from motifs II and III shown as bars. UniProt accession codes: wild-type 4Hpad-AE (Met1-Phe312; Q38HX2) and Pfl-AE (Met1-Phe255; POA9N4). **c** Cartoon representation of Pfl-AE (PDB code 3cb8; Ser11-Phe245). RS cluster shown as sticks coloured red for Fe and yellow for S. SAM shown as stick-and-ball with grey for C, red for O, blue for N and yellow for S. The T44-G47 loop (blue stick-and-ball) is the location for the putative ferredoxin-like domain insertion.

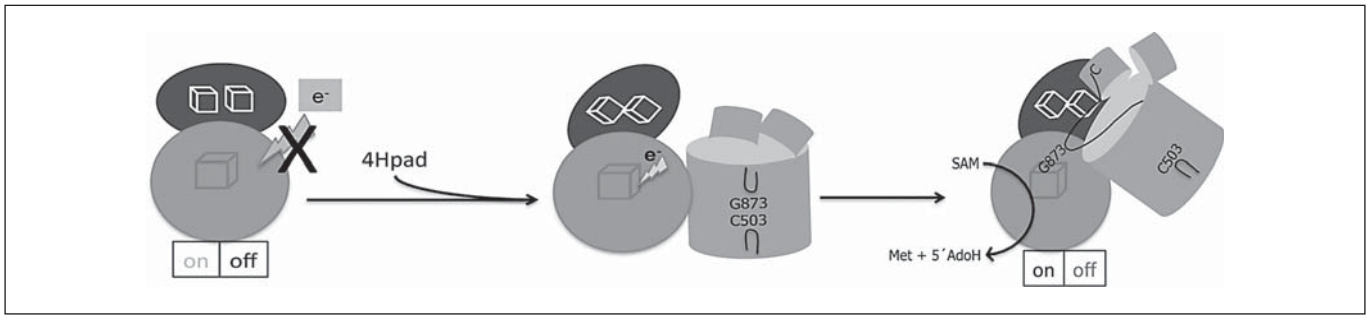

Fig. 2. Possible modes of action for 4Hpad-AE in vivo. Left panel: the ferredoxin-like domain (dark grey) downregulates the reactivity of the $[4Fe\text{-}4S]^{+2/+1}$ RS cluster in the absence of the decarboxylase. Middle panel: upon complex formation with decarboxylase, the RS cluster can be reduced to the $[4Fe\text{-}4S]^{+1}$ state. Right panel: SAM is reductively cleaved to the transient 5′-deoxyadenosyl radical that activates the decarboxylase by hydrogen atom abstraction at Gly873. The ferredoxin-like domain might contribute to a long-lasting glycyl radical by shielding the Gly873-containing loop from solvent during the activation process.

information on the transient complex derives from Pfl-AE in complex with SAM and a peptide substrate mimicking the glycine-containing loop of Pfl [Vey et al., 2008]. The structure shows the drastic conformational change that Pfl must undergo to make the glycine loop, buried 8 Å below the protein surface, accessible to the RS cluster of Pfl-AE. Pfl exists in equilibrium between a closed conformation with the glycine loop buried in the active site and an open conformation with the loop more solvent exposed and directly accessible to Pfl-AE [Peng et al., 2010]. By analogy, Selvaraj et al. [2014] proposed that the ferredoxin-like domain of 4Hpad-AE can shield the cysteine loop during its positioning near the RS cluster and, after the generation of the glycyl radical, the domain can help in protecting the loop from solvent during its reinsertion into the core of the decarboxylase (fig. 2). The experimental data support for these conjectures were derived from in vitro studies and so one cannot discard the alternative hypothesis that, in vivo, the auxiliary clusters might act as an electron conduit regulating the reactivity of the RS cluster in the absence of the decarboxylase.

Structural Characterization of 4Hpad

Crystal Structure of the Decarboxylase Component from C. scatologenes at 1.75 Å Resolution

The crystal structure of the decarboxylase provided the first structural information on a GRE containing Fe-S clusters [Martins et al., 2011]. 4Hpad is a functional $(\beta\gamma)_4$ heterotetramer (~440 kDa) comprising a 100-kDa catalytic β-subunit harbouring the glycyl/thiyl prosthetic group and a small 9.5-kD γ-subunit binding two [4Fe-4S] clusters [Martins et al., 2011; Yu et al., 2006]. Two βγ heterodimers, each comprising one β-subunit and one γ-subunit, were present in the asymmetric unit, and the crystal packing displayed a cloverleaf-shaped $(\beta\gamma)_4$ tetramer of heterodimers (fig. 3a). Two $(\beta\gamma)_2$ heterodimers build up the functional $(\beta\gamma)_4$ heterotetramer with dimensions of $125 \times 95 \times 76$ Å and a surface area of about 110,000 Å^2. The two molecular interfaces within the heterotetramer are solely formed by the β-subunit. One interface is built by interlocking the helices at the bottom of the $(\alpha/\beta)_{10}$ protein core barrel burying an area of 3,729 Å^2, and the second interface comprises helices surrounding the barrel burying an area of 1,739 Å^2. The βγ interface covers a total buried area of 3,471 Å^2, corresponding to 12% of the βγ heterodimer surface area and 6 and 30%, respectively, of the β- and γ-subunits. The C-terminal Fe-S cluster of the γ-subunit and two coordinating cysteines are directly involved in the βγ heterodimer interface. Both N- and C-terminal Fe-S clusters are at a distance of 40 Å apart from the active site and the inter-cluster distance is 20 Å.

Subunit Topology

The catalytic β-subunit displays the GRE canonical topology with a ten-stranded -α/β-barrel, $(\alpha/\beta)_{10}$, composed of two antiparallel five-stranded sheets surrounded by α-helices (fig. 3b, c). The α/β-barrel with an inner diameter of roughly 19 Å (distance between Cα atoms) forms a stable scaffold anchoring two β-hairpin loops opposite one another (fig. 3b). While one loop extends from the top of the barrel harbouring the storage radical at Gly873, the second loop protrudes from the bottom of the barrel and contains the catalytically active thiyl radical derived from Cys503. The glycyl/thiyl radical dyad prosthetic group displays two fingerprint sequences. Whereas Gly873 is inserted in an amino acid sequence (VRVA**G**FTQ) that slightly differs from the conserved GRE signature ([STIV]XR[IVT][CSA]**G**Y{GI}[GACV]; PROSITE: PDOC00665), Cys503 is within a sequence motif characteristic for each individual GRE (RA[WF][CA]LGG**C**LE[ST][AS]P for 4Hpad). The Gly873-containing loop, together with two neighbouring parallel helices at the C-terminal region, builds the radical domain.

The small γ-subunit comprises two domains with 28% amino acid sequence identity structurally related by a pseudo-2-fold symmetry, indicating a gene duplication origin (fig. 3d). Both domains display the same fold: a 3_{10}-helix perpendicular to three antiparallel β-strands (fig. 3e).

The N-terminal domain binds 1×[4Fe-4S] cluster with one histidine and three cysteines ($HX_2CX_{12}CX_{16}C$), and the C-terminal domain coordinates the second [4Fe-4S] cluster with four cysteines ($CX_3CX_{13}CX_{17}C$). Whereas the C-terminal cluster is buried in the βγ heterodimer interface, the N-terminal cluster is partially solvent accessible. When the crystal structure was published, the γ-subunit had no sequence similarity to any protein with known function, but the two domains showed structural similarity to high-potential iron-sulphur proteins (HiPIPs). Despite the weak amino acid sequence identity (13–18%), the cluster-binding motifs are remarkably similar, with $H/CX_2CX_{12-13}CX_{16-17}C$ for the γ-subunit and $CX_2CX_{13-19}CX_{14-19}C$ for HiPIPs. This observation led to the hypothesis that the two domains from the γ-subunit might have derived from a duplication of the HiPIPs cluster-binding scaffold [Martins et al., 2011].

Both Fe-S cluster-binding motifs found in the γ-subunit from 4Hpad (UniProt accession code Q38HX3) are present in the homologous sequence from *P. difficile*

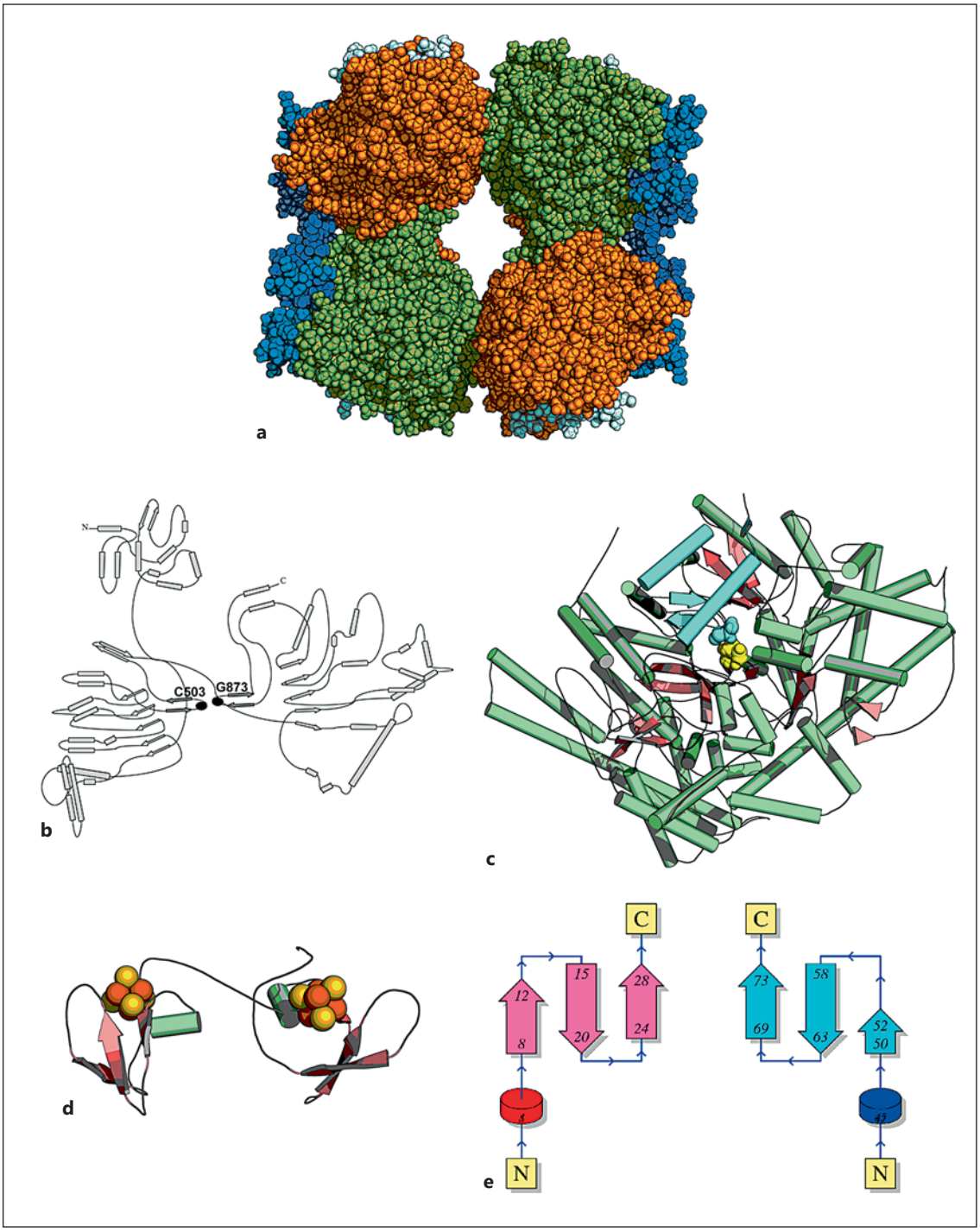

Fig. 3. Crystal structure of 4Hpad. **a** 4Hpad heterotetramer. Goodsell-like representation of the functional $(\beta\gamma)_4$ heterotetramer (~440 kD). The β-subunits are coloured as orange and green with the radical domain in cyan. The γ-subunits are coloured in light blue for N-terminal and in dark blue for C-terminal domains. **b** Plumbing diagram of the β-subunit. The 2 black dots indicate the location of the Cys503- and Gly873-containing loops. **c** Secondary structure elements of the β-subunit with α-helices in green, β-strands in salmon and the radical domain in cyan. Gly873 and Cys503 are shown as cyan and yellow spheres. **d** Secondary structure elements of the γ-subunit with 3_{10}-helices in green and β-strands in salmon. The 2 Fe-S clusters are in spheres with red for iron and yellow for sulphur. **e** Plumbing diagram of the N- and C-terminal domains of the γ-subunit.

($HX_2CX_{12}CX_{13}C$ and $CX_2CX_{13}CX_{17}C$; UniProt accession code Q84F15). A similar 4-cysteine sequence motif, $CX_2CX_{14-19}CX_{22-23}C$, is found in the β- and γ-subunits of BSS from *Thauera aromatica* (UniProt accession codes O87944 and O87942, respectively) and from *Azoarcus* sp. T (UniProt accession codes Q8VPT6 and Q8VPT8, respectively). At the time the crystal structure of BSS was unknown and a HiPIP-based origin for the β- and γ-subunits of BSS was hypothesized. This conjecture has recently been corroborated by the crystal structure of BSS [Funk et al., 2014].

Comparison of 4Hpad with GREs

Canonical GRE $(\alpha/\beta)_{10}$-Barrel Protein Fold

Currently, we have structural information on the catalytic subunits of class III Nrd (PDB code 1hk8) [Logan et al., 1999], Pfl (PDB code 1h16) [Becker et al 1999], GD (PDB code 1r9d) [O'Brien et al., 2004], Pfl2 (PDB code 2f3o) [Lethiö et al., 2006], 4Hpad (PDB code 2yaj) [Martins et al., 2011] and BSS (PDB code 4pkf) [Funk et al., 2014; Li et al., 2009]. As expected, all proteins share the GRE canonical topology: a ten-stranded tα/β-barrel consisting of two parallel five-stranded β-sheets arranged in an antiparallel manner, surrounded by α-helices (see fig. 3b for topology for 4Hpad). This fold was observed for the first time in class I Nrd protein R1 [Uhlin and Eklund, 1994], which does not belong to the GRE family. The inner diameter of the $(\alpha/\beta)_{10}$-barrel is significantly larger than the traditional $(\alpha/\beta)_8$-barrel (also called TIM-barrel), allowing the insertion of two opposite facing hairpin loops, bringing the cysteine/glycine prosthetic group in close vicinity (<5 Å). The glycine-containing loop together with two parallel neighbouring α-helices builds the radical domain (see fig. 3c for example in 4Hpad), which must undergo drastic conformational changes in order to give the RS cluster of the AE access to the glycine loop, deeply buried below the protein surface (16 Å in the case of 4Hpad) [Vey et al., 2008]. The radical domain is structurally conserved in all GREs except for Ndr, which instead displays a metal-binding domain [Logan et al., 2003].

Additional Structure Elements to the $(\alpha/\beta)_{10}$-Barrel

All characterized proteins display structural features in addition to the GRE canonical fold. 4Hpad has four regions. One segment (Met53-His85) contains a helix-turn-helix motif and is part of the β-β interface between two βγ heterodimer. This topology is conserved in GD, Pfl2 and BSS, but absent in Pfl and Ndr. A second feature comprising a helical region (Ser286-Gly313) is involved in the βγ heterodimer interface. This helical arrangement is conserved in BSS and partially present in GD and Pfl2. The two other features are predominantly coil regions (Gln121-Lys167 and Asn672-Glu700) surrounding the radical domain. Region Gln121-Lys167 is only partially present in GD and Pfl2. Notably, in BSS, part of the corresponding region is involved in the interface between catalytic and β-subunits. Region Asn672-Glu700 is partially present in GD and Pfl2, but absent in Ndr, Pfl and BSS.

Active Site Topology and Substrate-Binding Mode

In all structurally characterized GREs, we find the active site deeply embedded in the core of the $(\alpha/\beta)_{10}$-barrel. Figure 5 shows the comparison between the active site architecture from 4HPad and other GREs, with the respective substrate-binding mode when available. The active site pockets are, with the exception of Ndr, hydrophobic and upon substrate binding become compact by means of binding the respective substrates through extensive van der Waals contacts.

In 4Hpad [Martins et al., 2011], the active site pocket has a volume of roughly 1700 $Å^3$ and is only accessed through a funnel-shaped crevice spanning 24 Å from the molecular surface to Cys503. The putative glycyl radical storage site, Gly873, is located at distance of 4.7 Å from Cys503 and is not part of the active site pocket. In the substrate-free state, six water molecules, all at hydrogen-bonding distances from each other, tightly fill the void volume of the pocket. Upon substrate binding all solvent molecules are displaced and, notably, the location of five of the six water molecules is taken over by atoms of the substrate, with the carboxylate group substituting two water molecules sandwiched between Ser344 and Cys503, while the phenolic group replaces a water molecule adjacent to Glu637 (fig. 4a). Substrate binding induces a movement of the Gly873 loop towards Cys503. Except for the tripeptide Cys503-Glu505, all side chains at or within the active site pocket retain the same conformation observed in the substrate-free state. Cys503 shows an additional conformation and Glu505 is less clearly defined in the electron density map, with possible movement towards the carboxyl group of the substrate. In all structurally characterized GREs, the GlyCα to CysSγ interatomic distance ranges from 3.5 Å for Pfl with bound pyruvate (PDB code 1h16) to 5.2 Å for Ndr (Gly580A variant; PDB code 1hk8). BSS show an interatomic distance of 3.8 Å that increases to 4.4 Å in the absence of the γ-subunit (PDB codes 4pkc and 4pkf, respectively). For GD, the in-

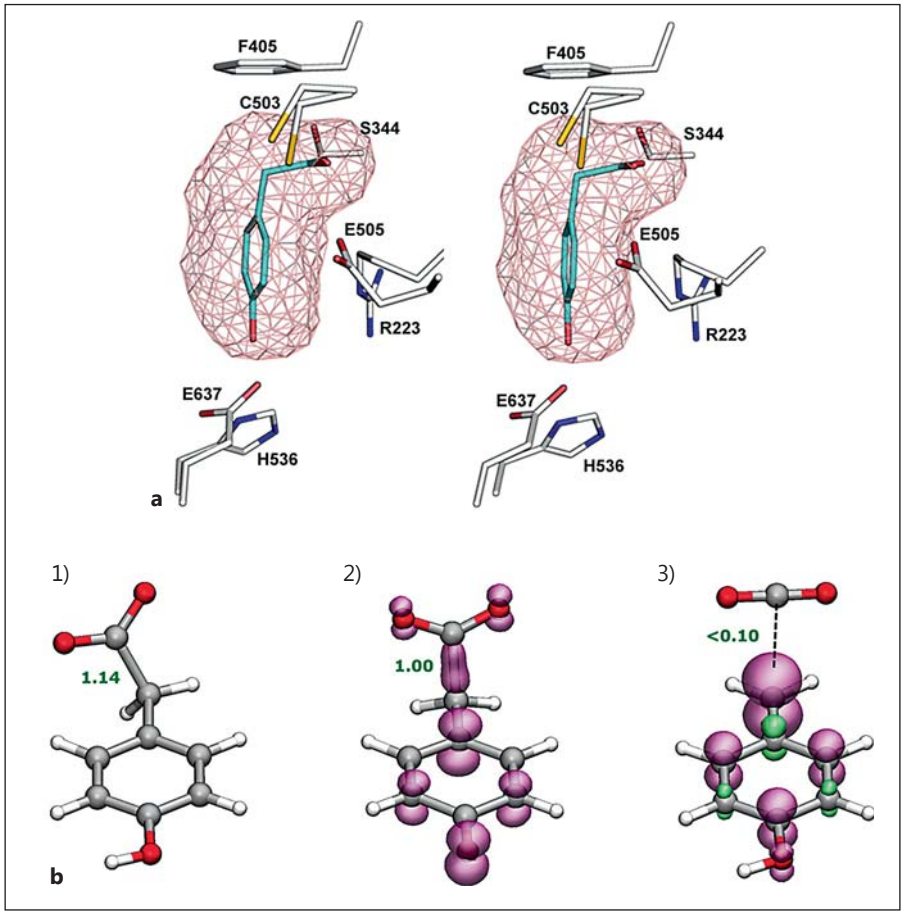

Fig. 4. 4-Hydroxyphenylacetate bound in the active site (**a**) and optimized geometries (**b**). **a** The atom colour is white for C (except for the substrate in cyan), red for O, blue for N and yellow for S. The pocket cavity is shown as salmon mesh. See text for details. **b** Panel 1: 4-hydroxyphenylacetate; panel 2: 4-Oxodobenzylcarboxyl radical; panel 3: 4-Hydroxbenzyl radical. Geometries calculated using the B3LYP functional and the 6-311++G(2d,2p) basis set. The volumes show the spin density distribution. The numbers indicate the Mayer bond-order parameter between the methylene carbon and the carboxylate carbon. Reprinted with permission from Feliks et al. [2013]. Copyright (2013) American Chemical Society. See text for details.

teratomic distance decreases from 4.4 Å in the substrate-free state to 4.1 Å with bound glycerol (PDB code 1r9d). Hence, a similar interatomic distance between the radical dyad cysteine/glycine is shared by all characterized GREs, corroborating the hypothesis that a radical could be generated on the cysteine residue through the short-range transfer of a hydrogen atom to the glycine residue [Logan et al., 1999].

The active site of 4Hpad is most similar to that of GD, with the carboxyl group from 4-hydroxyphenylacetate superimposing well with the C2-C3(OH) moiety of glycerol (fig. 5a). The active site volume of GD is reduced due to the side chains of Asp447 and Tyr640. A comparison with Pfl2 superimposes the carboxyl group with the C1-C2(OH) of glycerol (fig. 5b). The void volume of the active site is reduced through the side chains of Asp440, Tyr630 and Met632. A comparison with Pfl superimposes the carboxyl group with Cys418 (fig. 5c). Here, the side chains Phe432 and Trp333 contribute to a reduced void volume of the active site pocket. Arg176, structurally conserved with Arg223 in 4Hpad, anchors both the carboxyl and hydrated keto groups of pyruvate. There is no structural information on the substrate-binding mode for BSS (fig. 5d) and Ndr (fig. 5e).

A comparison of GREs in their substrate-free and substrate-bound states indicates that the active site in GREs has a 'ready-to-bind' scaffold, allowing substrate binding without substantial structural rearrangements.

Mechanism of 4-Hydroxyphenylacetate Decarboxylation

Clues from the Crystal Structure of the Substrate-Bound State of the Enzyme

The crystal structure of the substrate-bound state revealed an unexpected binding mode for 4-hydroxyphenylacetate, with the carboxyl group in close proximity to Cys503 and the phenolic hydroxyl anchored by Glu637 and His536 (fig. 5a) [Martins et al., 2011]. The substrate is

tightly bound in the active site through an extensive network of hydrogen-bonding interactions involving both the substrate carboxyl and hydroxyl groups. There are also van der Waals interactions between the substrate benzyl group and the side chains of aliphatic and aromatic amino acid residues, as well as a π-cation interaction between the aromatic ring and the guanidinium moiety of Arg223. These interactions serve to constrain the 4-hydroxyphenylacetate molecule such that the carboxymethyl moiety adopts a conformation that approximately occupies a plane perpendicular to the benzenoid ring (torsion angle ~100° between the benzenoid and carboxylate planes).

Because the substrate-bound state was obtained by crystal soaking instead of co-crystallization, doubts remained concerning the relevance of the observed mode of substrate binding. In order to corroborate the observed binding mode, the decarboxylase was co-crystallized with the physiological substrates 4-hydroxyphenylacetate and 3,4-dihydroxylphenylacetate and with the competitive inhibitor 4-hydroxyphenylacetamide (Selvaraj et al., unpubl. data). The three crystal structures confirm the previously observed substrate-binding mode [Martins et al., 2011]. Hence, the requirement for a phenolic hydroxyl group in the *para*-position of the substrate most probably complies with two requisites: (1) it anchors the substrate in the active site via hydrogen-bonding interactions involving Glu637 and His536 and (2) by deprotonation/back-protonation it favours first the formation of the intermediate *p*-benzoquinone methide radical anion (4-hydroxybenzyl radical) and afterwards the abstraction of a hydrogen atom from Cys503-SH, generating the product *p*-cresol and regenerating Cys503-S·.

The spontaneous loss of carbon dioxide from a substituted acetate ($XCH_2CO_2^- \rightarrow XCH_2^- + CO_2$) requires that X is an electron sink in order to stabilize the methylene carbanion resulting from heterolytic C-C bond cleavage. However, 4-hydroxyphenylacetate cannot undergo easy decarboxylation in this way owing to the high electron density in the aromatic ring. An 'Umpolung' of the aromatic ring was therefore postulated with the generation of radical intermediates via a one-electron oxidation mediated by either a flavin or an Fe-S cluster [Buckel and Golding, 1999]. This mechanism was revised after the characterization of the decarboxylase as a GRE, with the abstraction of a hydrogen atom from the phenolic hydroxyl by a cysteine thiyl radical being proposed as the initiating step [Selmer and Andrei, 2001]. This mechanism requires that the hydroxyl group is proximate to the catalytic cysteine residue, whereas the substrate-enzyme crystal structure showed that it is the carboxyl group that is close to this cysteine (fig. 6). This observation suggested a Kolbe-type decarboxylation, in which the role of the cysteine radical is to oxidize the carboxylate to a carboxyl radical, which fragments to carbon dioxide and a 4-hydroxybenzyl radical ($HOC_6H_4CH_2\cdot$) or a 4-oxidobenzyl radical ($^-OC_6H_4CH_2\cdot$). The near-parallel alignment of the orbitals of the C-C bond between the carboxylate and methylene carbon with the *p*-orbitals of the benzenoid ring, as observed in the bound substrate conformation (fig. 6), facilitates the decarboxylation.

In postulated mechanisms of GREs, the first step usually consists of a hydrogen atom abstraction from the substrate by the thiyl radical (Cys-S·), generating a substrate-derived radical and Cys-SH [Feliks and Ullmann, 2012; Frey, 2001; Frey et al., 2006]. With 4Hpad the reaction starts with Cys503-S· (thiyl radical) oxidizing the substrate carboxylate to a substrate-derived radical and a thiolate (Cys503-S^-) that can be protonated by Glu505 (at a distance of 3 Å from Cys503) to Cys503-SH. Thus, the electron transfer from the carboxylate to the thiyl radical and protonation of the resulting thiolate are coupled. The redox potential values (E_m vs. normal hydrogen electrode at pH 7) of 1.33 V for the pair ($Cys\text{-}S\cdot + H^+ + e^-$)/Cys-SH and 1.40 V for ($R\cdot + CO_2 + e^-$)/$R\text{-}COO^-$, with $R = C_6H_5$ [Komuro et al., 1995; Sasaki et al., 1966] make the proposed redox process thermodynamically feasible. The transfer of the radical from Cys503-S· to the substrate is followed by decarboxylation to the 4-hydroxybenzyl radical and CO_2. The removal of the phenolic proton by Glu637 and a π-cation interaction between the ring and the guanidinium moiety of Arg223 might further contribute to the resonance stabilization of the intermediate 4-oxidobenzyl radical (*p*-benzoquinone methide radical anion; $^-OC_6H_4CH_2\cdot + H^+ \rightleftarrows HOC_6H_4CH_2\cdot$) upon CO_2 elimination. The same radical intermediate was proposed to be involved in tyrosine scission during the formation of the CO and CN^- ligands of [Fe-Fe] hydrogenase and its catalytic relevance was recently demonstrated [Kuchenreuther et al., 2013]. The final step, protonation of the phenolate, is coupled with the abstraction of the hydrogen atom from Cys503-SH, yielding *p*-cresol and regenerating the thiyl radical Cys503-S·.

Computational Studies on the Mechanism of 4-Hydroxyphenylacetate Decarboxylation

The catalytic cycle was investigated by continuum electrostatics and quantum chemical/molecular mechanical calculations [Feliks et al., 2013]. However, the basic

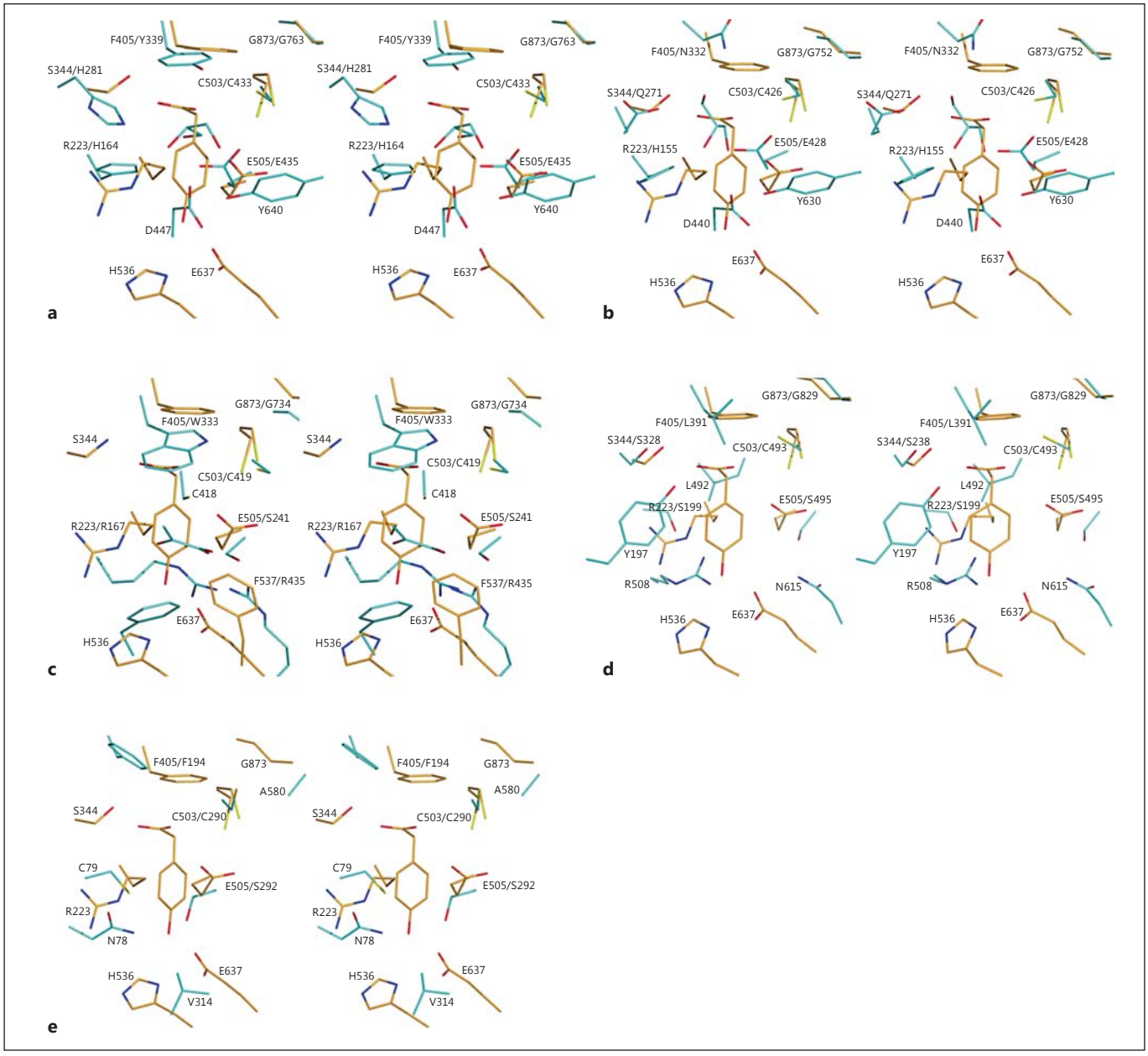

Fig. 5. Stereo views of active site architectures and of substrate-binding modes (when available) for GREs. The residue colour is blue for N, red for O and yellow for S. The carbon colour is orange for 4Hpad and cyan for other proteins. Residue labels are shown as 4Hpad/GRE. **a** Superposition with GD (PDB code 1r9d). Carboxylate group from 4-hydroxyphenylacetate superimposes with C2-C3(OH) moiety of glycerol. **b** Superposition with Pfl2 (PDB code 2f3o). Carboxylate group from 4-hydroxyphenylacetate superimposes with C1-C2(OH) moiety of glycerol. **c** Superposition with Pfl (PDB code 1h16). Carboxylate group from 4-hydroxyphenylacetate superimposes with Cys418. **d** Superposition with BSS (PDB code 4pkf). **e** Superposition with Ndr (PDB code 1h7a).

Fig. 6. Catalytic mechanism of 4Hpad. The chemical conversion steps of the substrate to the product are derived from quantum chemical calculations. Adapted with reprint permission from Feliks et al. [2013]. Copyright (2013) American Chemical Society. See text for details.

(For figure 6 see next page.)

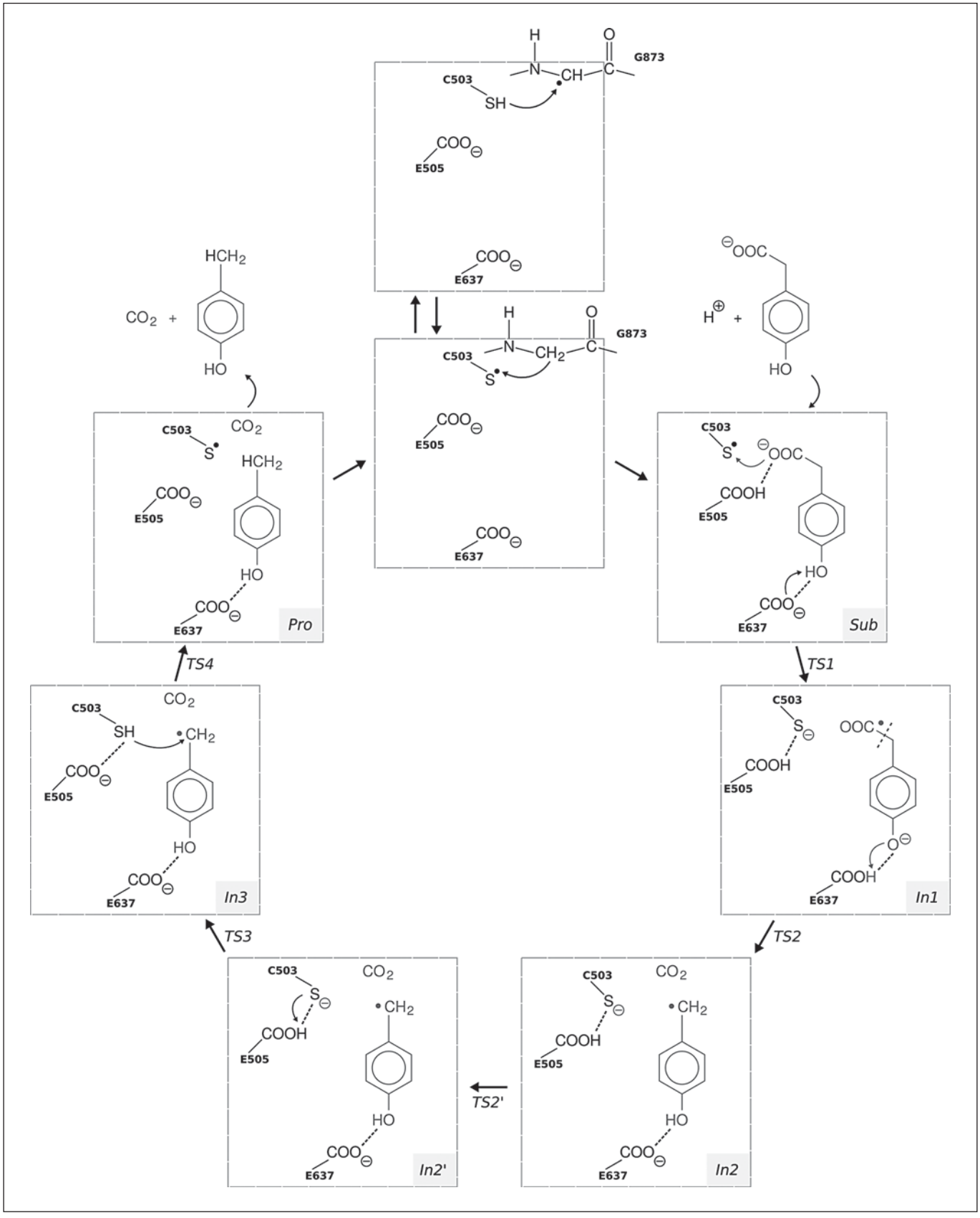
G873
C503
SH
E505
COO⊖
E637
CO2 +
HCH2
HO
CO2
S
HCH2
Pro
CH2
Sub
COOH
In3
In1
In2'
In2
TS1
TS2
TS2'
TS3
TS4

6

features of the catalytic mechanism can be already understood from simple quantum chemical calculations. A quantum chemical optimization of the substrate molecule 4-hydroxyphenylacetate gave a torsion angle for C2–C1–C7–C8 of ~120° (fig. 4b, panel 1). To mimic the formal hydrogen abstraction, an electron was removed from the molecule and the hydroxyl group was deprotonated to give the 4-oxidophenylacetate radical anion, which exhibited a torsion angle of ~90° after quantum chemical optimization (fig. 4b, panel 2). The protonation of the hydroxyl group of the 4-oxidophenylacetate radical anion followed by a new optimization lead to a geometry in which the distance between the methylene carbon atom and the carboxyl carbon is increased, leading to the release of carbon dioxide (fig. 4b, panel 3). Interestingly, the C2–C1–C7–C8 torsion angle of the substrate found in the crystal structure is ~100°, which indicates that the enzyme stabilizes the first transition state of the reaction.

The protonation state of active site residues was investigated by continuum electrostatic methods [Bashford and Karplus, 1990; Bombarda and Ullmann, 2010] using the software package GMCT [Ullmann and Ullmann, 2012]. The active site of 4Hpad contains several residues that can be protonated: Glu505 is located within a loop containing the cysteine thiyl radical, which is within hydrogen-bonding distance of both Cys503 and the carboxylate of 4-hydroxyphenylacetate. Glu637 is positioned at the opposite end of the active site and coordinates the hydroxyl group of the substrate by a hydrogen bond. His536 interacts closely with Glu637 and also with the hydroxyl group of the substrate. According to the calculations, Glu505 is protonated, Glu637 is deprotonated, and His536 is in its imidazolium form in the lowest energy protonation state at pH = 7. The positive charge on His536 is stabilized by the negatively charged Glu637. The calculations predict that the substrate binds in the active site with its carboxyl group deprotonated and its hydroxyl group protonated. The negative charge on the carboxylate is stabilized by a network of hydrogen bonds from Ser344, Glu505 (which is protonated) and a part of the protein backbone near Cys503. This protonation pattern was used as a starting point for a quantum mechanical/molecular mechanical analysis of the catalytic mechanism of 4Hpad [Feliks et al., 2013]. On the basis of the calculations, a five-step mechanism for the reaction was proposed (fig. 6). In the first step, the substrate 4-hydroxyphenylacetate is activated by an unusual concerted abstraction of an electron and a proton. Namely, the Cys503 thiyl radical abstracts an electron from the substrate and Glu637 abstracts a proton, which corresponds to the removal of a hydrogen atom in accordance with the general mechanism of GREs. In the second step, carbon dioxide readily splits off from the 4-hydroxyphenylacetate radical anion. The decarboxylation step is coupled to a proton transfer from the phenolic hydroxyl group to Glu637, which leads to the *p*-oxidobenzyl radical. The remaining steps of the reaction involve a rotation of the Cys503 side chain followed by a proton transfer from Glu505 to Cys503 and a hydrogen atom transfer from Cys503 to the *p*-oxidobenzyl radical to form *p*-cresolate. The calculated mechanism agrees with experimental data suggesting that both Cys503 and Glu637 are essential for the catalytic function of 4Hpad and that the substrate requires a hydroxyl group *para* to the acetate moiety (Selvaraj et al., unpubl. data).

Conclusions

4Hpad is physiologically active as a $(\beta\gamma)_4$ heterotetramer of 440 kD and uses an unprecedented Kolbe-type decarboxylation [Feliks et al., 2013; Martins et al., 2011] to catalyse the last step in the fermentative production of the bacteriostatic *p*-cresol (4-methylphenol) from tyrosine in *Clostridia* [D'Ari and Baker, 1985; Yu et al., 2006]. 4Hpad and BSS (reviewed in the same issue) are the prototype for a more complex GRE subclass in which the canonical HiPIP cluster-binding topology was, in the case of 4Hpad, duplicated and specifically modified to generate the γ-subunit, and in the case of BSS copied twice and further edited to generate the two β- and γ-subunits [Heider et al., this issue, pp. 29–44]. The additional Fe-S cluster containing subunit(s) in 4Hpad and BSS most probably represent a gain of function for this GRE subclass, allowing the host organisms to evolve regulatory mechanisms for an efficient response to environmental changes to achieve maximal ability to thrive.

4Hpad-AE uses S-adenosylmethionine (SAM or AdoMet) and a differentiated $[4Fe\text{-}4S]^{2+/+}$ cluster (RS cluster) to generate a stable glycyl radical on the decarboxylase [Selvaraj et al., 2013]. The auxiliary [4Fe-4S] clusters coordinated by a ferredoxin-like domain [Selvaraj et al., 2013] are not necessary for SAM-dependent glycyl radical generation in the decarboxylase but are vital for generating a persistent radical [Selvaraj et al., 2014]. The mechanism(s) contributing to or responsible for the stabilization effect are currently unknown and must await further characterization. In the absence of biochemical and structural information on other ferredoxin-like domain-containing GRE-AEs, one can only conjecture that the observed stabilization effect might be shared within the family.

Acknowledgements

We thank Matthias Boll and Rainer Meckenstock for the excellent organization of the Priority Programme SPP 1319 'Biological transformations of hydrocarbons in the absence of oxygen' funded by the Deutsche Forschungsgemeinschaft (DFG). W.B. and B.T.G. also thank the COST Action CM1201 Program (Biomimetic Radical Chemistry) for its support. We are grateful to T. Selmer (FH Aachen Campus Jülich) for the decarboxylase expression clone, S. Steinborn and R. Dietrich (Humboldt-Universität zu Berlin) for their technical assistance and all members of the SBBC Group for helpful discussions and continuous support.

References

Altschul SF, Madden TL, Schaffer AA, Zhang JH, Zhang Z, Miller W, Lipman DJ: Gapped BLAST and PSI-BLAST: a new generation of protein database search programs. Nucleic Acids Res 1997;25:3389–3402.

Andrei PI, Pierik AJ, Zauner S, Andrei-Selmer LC, Selmer T: Subunit composition of the glycyl radical enzyme p-hydroxyphenylacetate decarboxylase. A small subunit, HpdC, is essential for catalytic activity. Eur J Biochem 2004;271:2225–2230.

Bammens B, Evenepoel P, Keuleers H, Verbeke K, Vanrenterghem Y: Free serum concentrations of the protein-bound retention solute p-cresol predict mortality in hemodialysis patients. Kidney Int 2006;69:1081–1087.

Bashford D, Karplus M: Pkas of ionizable groups in proteins – atomic detail from a continuum electrostatic model. Biochemistry 1990;29:10219–10225.

Becker A, Fritz-Wolf K, Kabsch W, Knappe J, Schultz S, Wagner AFV: Structure and mechanism of the glycyl radical enzyme pyruvate formate-lyase. Nat Struct Biol 1999;6:969–975.

Bennett BD, Kimball EH, Gao M, Osterhout R, Van Dien SJ, Rabinowitz JD: Absolute metabolite concentrations and implied enzyme active site occupancy in *Escherichia coli*. Nat Chem Biol 2009;5:593–599.

Bombarda E, Ullmann GM: pH-dependent pK_a values in proteins – a theoretical analysis of protonation energies with practical consequences for enzymatic reactions. J Phys Chem B 2010;114:1994–2003.

Buckel W: Radical and electron recycling in catalysis. Angew Chem Int Ed Engl 2009;48:6779–6787.

Buckel W, Golding BT: Radical species in the catalytic pathways of enzymes from anaerobes. FEMS Microbiol Rev 1999;22:523–541.

D'Ari L, Barker HA: *p*-Cresol formation by cell-free extracts of *Clostridium difficile*. Arch Microbiol 1985;143:311–312.

Dawson LF, Stabler RA, Wren BW: Assessing the role of *p*-cresol tolerance in *Clostridia difficile*. J Med Microbiol 2008;57:745–749.

Demick JM, Lanzilotta WN: Radical SAM activation of the B_{12}-independent glycerol dehydratase results in formation of 5′-deoxy-5′-(methylthio)adenosine and not 5′-deoxyadenosine. Biochemistry 2011;50:440–442.

Dey A, Peng Y, Broderick WE, Hedman B, Hodgson KO, Broderick JB, Solomon EI: S K-edge XAS and DFT calculations on SAM dependent pyruvate formate-lyase activating enzyme: nature of interaction between the Fe4S4 cluster and SAM and its role in reactivity. J Am Chem Soc 2011;133:18656–18662.

Eklund H, Fontecave M: Glycyl radical enzymes: a conservative structural basis for radicals. Structure 1999;7:257–262.

Elsden SR, Hilton MG, Waller JM: End products of metabolism of aromatic amino acids by *Clostridia*. Arch Microbiol 1976;107:283–288.

Feliks M, Martins BM,Ullmann GM: Catalytic mechanism of the glycyl radical enzyme 4-hydroxyphenylacetate decarboxylase from continuum electrostatic and QC/MM calculations. J Am Chem Soc 2013;135:14574–14585.

Feliks M, Ullmann GM: Glycerol dehydratation by the B_{12}-independent enzyme may not involve the migration of a hydroxyl group: a computational study. J Phys Chem B 2012;116:7076–7087.

Frey PA: Radical mechanisms of enzymatic catalysis. Annu Rev Biochem 2001;70:121–148.

Frey PA, Hegeman AD, Reed GH: Free radical mechanisms in enzymology. Chem Rev 2006;106:3302–3316.

Frey PA, Hegeman AD, Ruzicka FJ: The radical SAM superfamily. Crit Rev Biochem Mol Biol 2008;43:63–88.

Funk MA, Judd ET, Marsh ENG, Elliott SJ, Drennan, CL: Structures of benzylsuccinate synthase elucidate roles of accessory subunits in glycyl radical enzyme activation and activity. Proc Natl Acad Sci USA 2014;111:10161–10166.

Gambarelli S, Luttringer F, Padovani D, Mulliez E, Fontecave M: Activation of the anaerobic ribonucleotide reductase by S-adenosylmethionine. Chem Biochem 2005;6:1960–1962.

Goldman PJ, Grove TL, Sites LA, McLaughlin MI, Booker SJ, Drennan, CL: X-ray structure of an AdoMet radical activase reveals an anaerobic solution for formylglycine posttranslational modification. Proc Natl Acad Sci USA 2013;110:8519–8524.

Hafiz S, Oakley CL: *Clostridium difficile* – isolation and characteristics. J Med Microbiol 1976;9:129–136.

Hioe, J, Savasci G Brand H, Zipse H: The stability of Cα peptide radicals: why glycyl radical enzymes? Chemistry 2011;17:3781–3789.

Knappe J, Neugebauer FA, Blaschkowski HP, Gänzler M: Post-translational activation introduces a free radical into pyruvate formate-lyase. Proc Natl Acad Sci USA 1984;81:1332–1335.

Komuro M, Higuchi T, Hirobe M: Application of chemical cytochrome P-450 model systems to studies on drug metabolism-VIII. Novel metabolism of carboxylic acids via oxidative decarboxylation. Bioorg Med Chem 1995;3:55–65.

Kuchenreuther JM, Myers WK, Stich TA, George SJ, Nejatyjahromy Y, Swartz JR, Britt RD: A radical intermediate in tyrosine scission to the CO and CN^- ligands of Fe-Fe hydrogenase. Science 2013;342:472–475.

Lanz ND, Booker SJ: Identification and function of auxiliary iron-sulfur clusters in radical SAM enzymes. Biochim Biophys Acta 2012;1824:1196–1212.

Lehtiö L, Grossmann JG, Kokona B, Fairman R, Goldman A: Crystal structure of a glycyl radical enzyme from *Archaeoglobus fulgidus*. J Mol Biol 2006;357:221–235.

Leuthner B, Leutwein C, Schulz H, Horth P, Haehnel W, Schiltz E, Schagger H, Heider J: Biochemical and genetic characterization of benzylsuccinate synthase from *Thauera aromatica*: a new glycyl radical enzyme catalysing the first step in anaerobic toluene metabolism. Mol Microbiol 1998;28:615–628.

Li L, Patterson DP, Fox CC, Lin B, Coshigano PW, Marsh ENG: Subunit structure of benzylsuccinate synthase. Biochemistry 2009;48:1284–1292.

Logan DT, Andersson J, Sjoberg BM, Nordlund P: A glycyl radical site in the crystal structure of a class III ribonucleotide reductase. Science 1999;283:1499–1504.

Logan DT, Mulliez E, Larsson KM, Bodevin S, Atta M, Garnaud PE, Sjoberg BM, Fontecave M: A metal-binding site in the catalytic subunit of anaerobic ribonucleotide reductase. Proc Natl Acad Sci USA 2003;100:3826–3831.

Martins BM, Blaser M, Feliks M, Ullmann GM, Buckel W, Selmer T: Structural basis for a Kolbe-type decarboxylation catalyzed by a glycyl radical enzyme. J Am Chem Soc 2011;133:14666–14674.

O'Brien JR, Raynaud C, Croux C, Girbal L, Soucaille P, Lanzilotta WN: Insight into the mechanism of the B_{12}-independent glycerol dehydratase from *Clostridium butyricum*: preliminary biochemical and structural characterization. Biochemistry 2004;43:4635–4645.

Ollagnier S, Mulliez E, Schmidt PP, Eliasson R, Gaillard J, Deronzier C, Bergman T, Graslund A, Reichard P, Fontecave M: Activation of the anaerobic ribonucleotide reductase from *Escherichia coli*. The essential role of the iron-sulfur center for S-adenosylmethionine reduction. J Biol Chem 1997;272:24216–24223.

Peng Y, Veneziano SE, Gillispie GD, Broderick JB: Pyruvate formate-lyase, evidence for an open conformation favored in the presence of its activating enzyme. J Biol Chem 2010;285:27224–27231.

Poveda J, Sanchez-Nino MD, Glorieux G, Sanz AB, Egido J, Vanholder R, Ortiz A: *p*-Cresyl sulphate has pro-inflammatory and cytotoxic actions on human proximal tubular epithelial cells. Nephrol Dial Transplant 2014;29:56–64.

Sasaki K, Uneyama K, Nagura S: An energetic explanation of the Kolbe electrosynthesis. Electrochim Acta 1966;11:891–894.

Selmer T, Andrei PI: *p*-Hydroxyphenylacetate decarboxylase from *Clostridium difficile*. A novel glycyl radical enzyme catalysing the formation of *p*-cresol. Eur J Biochem 2001;268:1363–1372.

Selmer T, Pierik AJ, Heider J: New glycyl radical enzymes catalysing key metabolic steps in anaerobic bacteria. Biol Chem 2005;386:981–988.

Selvaraj B, Pierik AJ, Bill E, Martins BM: 4-Hydroxyphenylacetate decarboxylase activating enzyme catalyses a classical S-adenosylmethionine reductive cleavage reaction. J Biol Inorg Chem 2013;18:633–643.

Selvaraj B, Pierik AJ, Bill E, Martins BM: The ferredoxin-like domain of the activating enzyme is required for generating a lasting glycyl radical in 4-hydroxyphenylacetate decarboxylase. J Biol Inorg Chem 2014;19:1317–1326.

Shisler KA, Broderick JB: Glycyl radical activating enzymes: structure, mechanism, and substrate interactions. Arch Biochem Biophys 2014;546:64–71.

Sofia HJ, Chen G, Hetzler BG, Reyes-Spindola JF, Miller NE: Radical SAM, a novel protein superfamily linking unresolved steps in familiar biosynthetic pathways with radical mechanisms: functional characterization using new analysis and information visualization methods. Nucleic Acids Res 2001;29:1097–1106.

Stone RW, Machamer HE, Mcaleer WJ, Oakwood TS: Fermentation of tyrosine by marine bacteria. Arch Biochem 1949;21:217–223.

Uhlin U, Eklund H: Structure of ribonucleotide reductase protein R1. Nature 1994;370:533–539.

Ullmann RT, Ullmann GM: GMCT: A Monte Carlo simulation package for macromolecular receptors. J Comp Chem 2012;33:887–900.

Vey JL, Yang J, Li M, Broderick WE, Broderick JB, Drennan CL: Structural basis for glycyl radical formation by pyruvate formate-lyase activating enzyme. Proc Natl Acad Sci USA 2008;105:16137–16141.

Wong KK, Murray BW, Lewisch SA, Baxter MK, Ridky TW, Ulissidemario L, Kozarich JW: Molecular properties of pyruvate formate-lyase activating enzyme. Biochemistry 1993;32:14102–14110.

Yang J, Naik SG, Ortillo DO, Garcia-Serres Li RM, Broderick WE, Huynh HB, Broderick JB: The iron-sulfur cluster of pyruvate formate-lyase activating enzyme in whole cells: cluster interconversion and a valence-localized $[4Fe\text{-}4S]^{2+}$ state. Biochemistry 2009;48:9234–9241.

Yokoyama MT, Carlson JR: Production of skatole and *para*-cresol by a rumen *Lactobacillus* Sp. Appl Environ Microbiol 1981;41:71–76.

Yu L, Blaser M, Andrei PI, Pierik AJ, Selmer T: 4-Hydroxyphenylacetate decarboxylases: properties of a novel subclass of glycyl radical enzyme systems. Biochemistry 2006;45:9584–9592.